JOURNAL OF MATERIALS SCIENCE 27 (1992) 215–225

Planar-flow spin-casting of molten metals: process behaviour

J. K. CARPENTER
Modifiers Research Department, Rohm and Haas Company, Bristol, PA 19007, USA
P. H. STEEN*
School of Chemical Engineering, Cornell University, Ithaca, NY 14853, USA

An experimental study of the planar-flow melt-spinning process was performed in order to gain a better understanding of the steady-state production of microcrystalline and amorphous ribbons. The dependence of the thickness of the ribbon product, T, on process parameters (wheel speed, U, nozzle/wheel gap, G, overpressure, ΔP, nozzle-slot breadth, R, and nozzle-slot width, W) was determined using an apparatus designed to deliver reproducible results. Thicknesses were reproducible to within 5%–8%. Guided by dimensional analysis, the non-dimensional thickness (T/G) was found to depend, within the experimental error, only on a non-dimensional pressure drop ($\Delta P/\rho U^2$) and slot breadth (R/G) for fixed thermal conditions. Data from the literature and our data, which considerably extend the range, correlate consistently on this basis. In contrast to the steady behaviour, the limits within which a uniform ribbon can be formed depend on a larger set of parameters; this dependence is sketched with the available data. Finally, a variety of observed ribbon surface textures (free meniscus side) is catalogued.

1. Introduction

Spin-casting of metals has been studied extensively as a continuous method of rapidly quenching amorphous or microcrystalline materials [1, 2]. In particular, the planar-flow configuration, patented by Narsimhan [3], has attracted a large amount of interest because of its capability of casting relatively wide ribbons of metal. Most previous work on the process, though, focused mainly on the microstructure and properties of the final product and not the metal processing. In addition, among the relatively few process studies, even fewer are based on experiment. Studies that have been performed include those by Takayama and Oi [4], Huang [5], Huang and Fiedler [6], Fiedler *et al.* [7], and Smith and Saletore [8].

A schematic illustration of the planar-flow melt-spinning process is shown in Fig. 1. To eject the molten metal from the nozzle, an applied pressure drop is necessary. As the metal is solidified, it is held between the hot nozzle face and cold chill wheel by surface tension. The ribbon of solidified metal is drawn out from beneath the metal puddle by the spinning wheel. A photograph of the spinner with ribbon spinning off is shown in Fig. 2.

Commercially available melt-spinners are typically unable to deliver ribbon thicknesses reproducible to better than 20%. The greatest technical difficulty in the experiments is the precise control and measurement of the nozzle/wheel gap. We have improved conventional techniques to achieve better reproducibility. Because of its relevance to the results, the custom design of the apparatus is first described in some detail.

To understand the results of the experiments it is useful to distinguish steady-state process behaviour from process stability. Only under certain conditions is a uniform ribbon observed to form. For example, if the overpressure is sufficiently high, the upstream molten metal meniscus will blow out spraying metal droplets to cool in the ambient air.

Charting (or predicting) these operating limits (stability boundaries) in the parameter space is of vital importance to commercialization. It is clear that the blow-out instability will depend on the particular metal or alloy under consideration through its surface tension. On the other hand, when the surface tension is sufficient to prevent the "blow-out" instability (and other instabilities are avoided) the thickness of the resulting ribbon may not be expected to depend on surface tension (and does not, as reported below). In this way, it is clear that the operating limits will generally involve more parameters than the steady-state behaviour. Dimensional analysis guides (reduces) the choice of relevant parameters. The elementary physical considerations which further restrict the relevant dimensionless groups for both the steady-state and stability issues are described.

Because of the fewer parameters involved the steady-state behaviour is easier to map out experimentally than the stability boundaries. After giving a sense of the reproducibility of our system, the dependence of the thickness on process variables is described

* *Author to whom correspondence should be addressed.*

0022–2461/92 $03.00 + .12

and the "power-law" correlation

$$T/G = a(\Delta P/\rho U^2)^b \quad (1)$$

is presented. The exponent b is found to vary $0.26 \leqslant b \leqslant 0.31$ depending on the slot-breadth (R/G). The results are then placed within the context of data from the literature.

Only a sketch of the operating limits is possible due to the large number of parameters involved. Nevertheless, the windows of system stability can begin to be discerned. These complete the report of quantitative results.

Qualitative observations of the process behaviour and a catalogue of descriptive sketches of ribbon textures round out the discussion.

2. Experimental procedure

2.1. Apparatus design

A general schematic view of the apparatus is shown in Fig. 3. The description of the apparatus is broken into three parts: wheel and motor, furnace and positioner, and crucible and nozzle. The instruments used to measure the process parameters are then described.

The chill wheel in this system is a drum made from a cylinder of copper/beryllium sandwiched between two side-plates of aluminium and mounted concentrically on a shaft. Maintenance of a small, approximately constant gap between the spinning wheel and nozzle face is the central goal of the design. The copper/beryllium rim is 61 cm diameter to minimize the curvature effects of the wheel. Curvature of the wheel changes the gap size 0.04 mm over a length of 1/2 cm, a typical length of the molten puddle. The concentricity of the wheel is such that the radius varies by $\pm$ 0.064 mm along its circumference. The changes in gap size due to the curvature and concentricity of the wheel are less than 6% of the typical gap size. The rim is 12.7 mm thick. Conservative estimates of the heat transfer from the molten metal show temperature changes reach no further than 1 mm into the wheel for a typical contact time between the metal and wheel, making the rim an essentially semi-infinite heat sink. The wheel speed is controlled between 100 and 500 r.p.m. to the nearest 1 r.p.m.

A 40 kW induction heater is used to heat the metal. The heating coil is made of 3/8 in. ($\sim$ 0.95 cm) copper tubing and was 20 cm high and 20 cm diameter. A fibreglass sheath is placed around the coil to help prevent arcing.

The heating coil is placed in a furnace made of ceramic board and fused quartz plates which hold the crucible and metal sample during the experiment. The ceramic boards make up the four sides of the furnace and the two quartz plates make up the bottom. The quartz is necessary for the bottom section of the

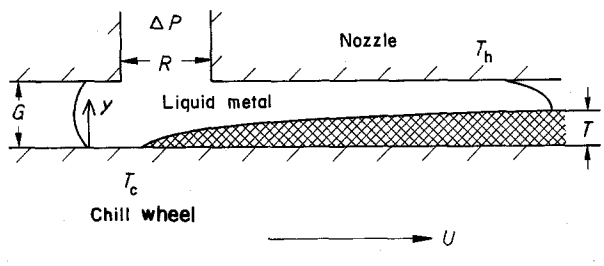

Figure 1 Schematic illustration of the planar-flow process.

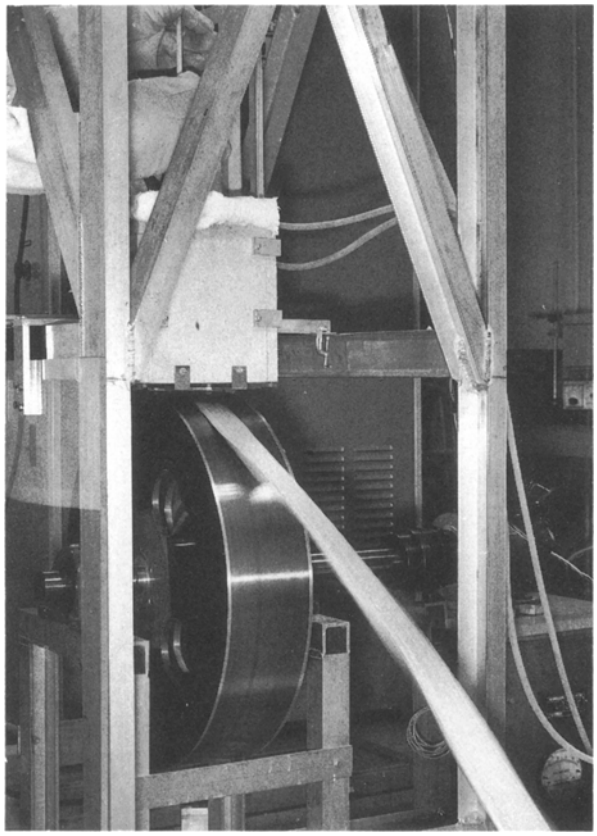

Figure 2 The planar-flow apparatus.

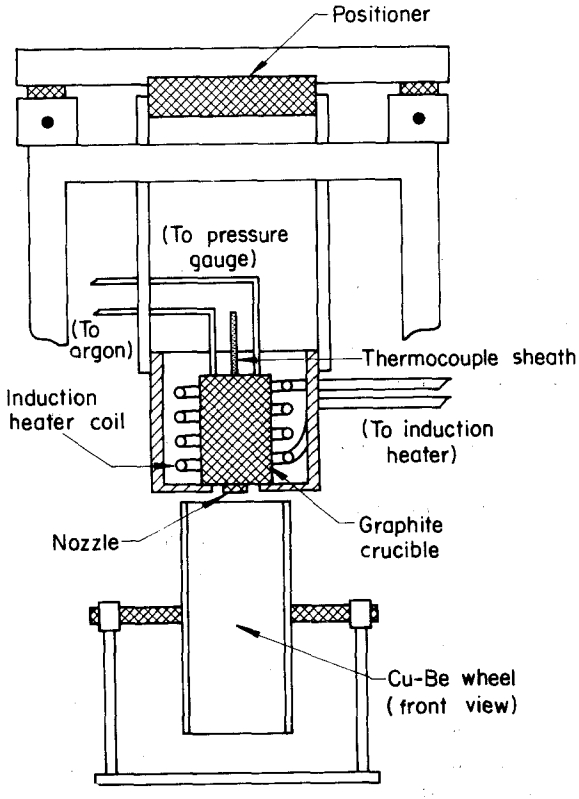

Figure 3 Schematic illustration of the planar-flow apparatus.

furnace because it does not bend as much as the ceramic under the weight of the crucible, and it maintains the nozzle at a fixed distance from the spinning wheel even during the continuous change in weight of the crucible that occurs as liquid metal is ejected.

A positioning unit supported by an aluminium framework is used to adjust the distance between the nozzle face and the spinning wheel. To ensure that changes in the bending of the aluminium channel cause no significant change in gap size when the molten metal is ejected, the framework is designed such that all beam deflections due to the weight of the metal are no greater than 10 μm.

Micropositioning devices used in the positioning unit give three linear degrees of freedom to the nozzle face and one rotational degree of freedom. Two vertical positioners support a cross beam to which the furnace is connected. This allows vertical movement of the nozzle and rotation about the axis parallel to the direction of casting. The connection to the crossbeam includes a horizontal positioner and a carriage attachment which allows two-dimensional movement of the nozzle in the plane parallel to the floor. A photograph of the framework and positioner (top) with furnace, crucible and nozzle in place is shown in Fig. 4.

The crucibles and nozzles are made from graphite. The space inside the crucible is 10 cm diameter and 23 cm high. The crucible is large enough to hold 2.25 kg aluminium, which ensures that the process is semi-continuous. However, results reported are from runs of 0.9 or 1.8 kg metal. The bottom of the crucible is threaded so that different nozzles may be interchanged from run to run. The nozzles are machined with slot breadths of 1590 or 3180 μm and slot widths of 25.4, 50.8 and 76.2 mm. To reduce the amount of burning of the graphite at high temperatures, the crucibles and nozzles are coated with a graphite coverguard. A photograph of the crucible and nozzle is shown in Fig. 5.

A constant overpressure of argon in the crucible, necessary for ejection of the metal, is maintained using a plunger-type system. A 3.81 cm diameter hole in the bottom of the crucible is lined with a 0.635 cm thick collar of boron nitride. A 2.54 cm diameter boron nitride plug, cemented to an aluminium oxide sheath, seals the hole while the sample is melting. The other end of the sheath protruded through the crucible cap, and the gap between the hole in the cap and the sheath is sealed by an O-ring. Argon is fed into the top of the crucible at a prescribed pressure. After pressurizing the crucible chamber, the boron-nitride plug is raised out of the hole when the metal is ready to be quenched. The gloves in Fig. 2 have raised this plug.

Most process parameters are measured directly. A pressure gauge is attached to the top of the crucible and the gauge measures the overpressure of argon to the nearest 0.64 cm (1/4 in.) water. A K-type thermocouple is placed in the aluminium oxide sheath attached to the boron nitride plug, and the temperature of the heated material is measured to the nearest degree Kelvin. The speed of the wheel is measured by a magnetic proximity switch and a digital tachometer displays the wheel speed to the nearest r.p.m.

To measure the gap between the nozzle face and the spinning wheel an indirect, optical method is employed. The nozzle/wheel gap is first measured with a feeler

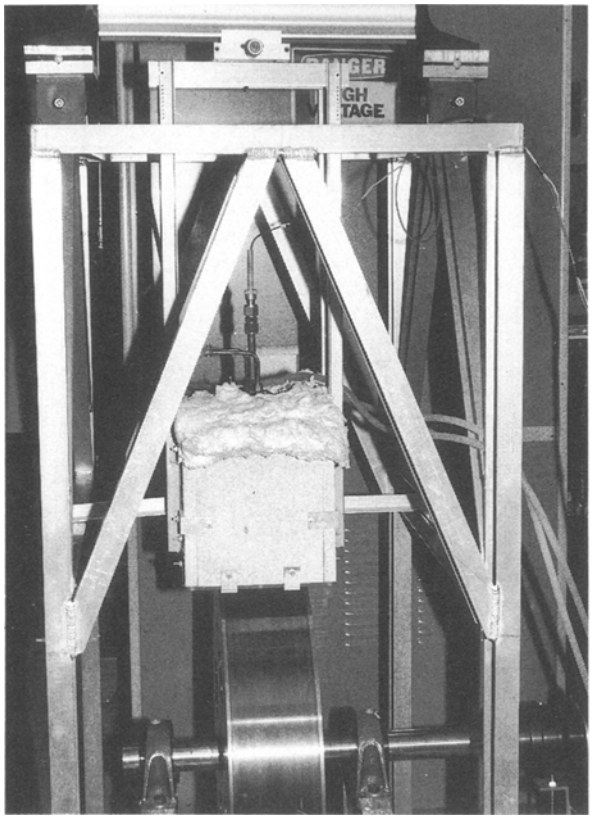

Figure 4 Positioner and framework.

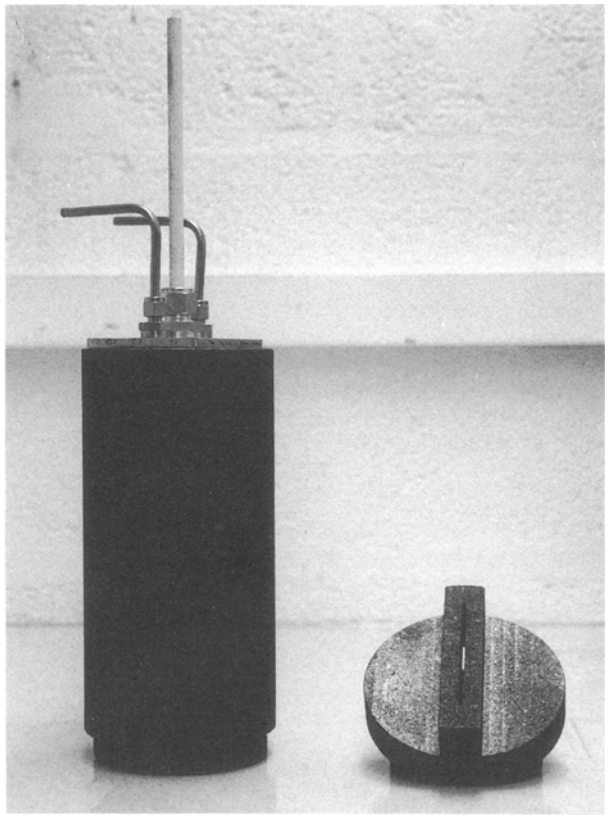

Figure 5 Crucible and nozzle.

gauge before the heating of the metal has started. A cathetometer is used to make a reference measurement of the gap length with the nozzle cold. During heating of the metal the gap is measured periodically with the cathetometer and as the nozzle expands due to heating, the positioning unit is adjusted to keep the gap size within 5% of the reference length. The size of the gap during the run is determined through proportionality, using the gap size determined by the feeler gauge when the nozzle is cold and the reference measurements made with the cathetometer when the nozzle is hot and cold.

2.2. Procedure and data analysis

Nominally pure aluminium metal is used in the experiments. The metal sample is loaded into the crucible and furnace. After attaching the nozzle to the crucible, the crucible, nozzle, metal sample, aluminium oxide sheath, and crucible cap are placed in the furnace box. The induction heater is turned on and the metal is heated until molten. After the metal is melted but before it is ejected, the wheel speed and argon pressure are set to their predetermined values for the experiment. The induction heater is turned off once the metal is superheated 100 K, and the run begins as the plunger is lifted to let the metal out (cf. Fig. 1). Including preparation, clean-up, and measurement of thickness, a typical run takes 10 h.

The dimensional results obtained from this system are listed in Table I. In contrast to the wheel speed and gap size, which are taken directly from the measurements on the system, the pressure drop is adjusted to account for the head of liquid metal. This pressure accounts for 10%–30% of the total pressure drop across the system at the start of the run. In analysing the data, the pressure drop is assumed to be the average of the pressure including the head of metal (i.e. before ejection) and the pure argon overpressure without the head of metal (i.e. just before the last bit of metal escapes). In determining the steady-state pressure for the extended runs (i.e. runs in which heat-up of the wheel did not allow all of the metal to form a uniform ribbon) the head of liquid metal is averaged for only the first half of the run, when the uniform product was produced.

The thickness of the ribbon is determined by an average weight. The length of the ribbon in a typical run is about 3 m. The first and last parts of the ribbon leaving the wheel, approximately 10% of all the metal solidified, are discarded because of nonuniformities due to transient effects. To determine a thickness for the ribbon, ten evenly spaced samples are taken along the ribbon length and weighed. An average thickness for each sample is determined from the mass based on the known length and width. The thicknesses determined from the ten runs are averaged to determine a mean thickness. Although the thickness changes slightly from sample to sample along the length of the ribbon, this change is not large. The standard deviation of the sample thicknesses is approximately 10% of the mean thickness. Typical ribbon thickness distributions about the mean are shown in Fig. 6.

3. Dimensional analysis and physical considerations

3.1. Steady-state dependence

Typical values for the geometry, process variables, and material properties corresponding to the process (Fig.

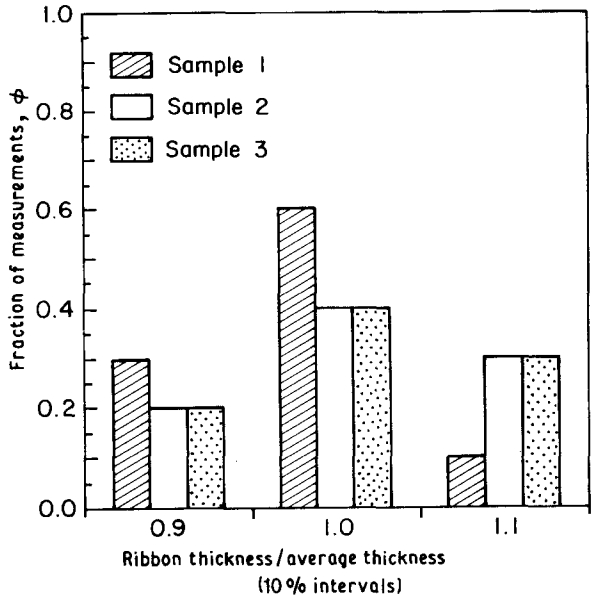

Figure 6 Ribbon thickness deviation plot.

TABLE I Typical values of process parameters

Dimensional parameters		Derived dimensionless groups	
Process parameters			
$R = 3.2 \times 10^{-3}$ m	Nozzle-slot breadth	Re ($\equiv \rho_l UG/\mu$) = 11 500	Reynolds number
$W = 5.1 \times 10^{-2}$ m	Nozzle-slot width	Wb ($\equiv \rho_l U^2 G/(2\sigma)$) = 67	Weber number
$G = 5.0 \times 10^{-4}$ m	Nozzle–wheel gap	ΔP ($\equiv \Delta P/(\rho_l U^2)$) = 0.022	Pressure drop/inertial forces
$T = 1.5 \times 10^{-4}$ m	Ribbon thickness	H ($\equiv H^*/U$) = 0.026	Average solidification slope
$H^* = 26$ cm s^{-1}	Average solidification rate	W ($\equiv W/G$) = 100	Slot width/nozzle–wheel gap
$U = 10$ m s^{-1}	Linear wheel speed	R ($\equiv R/G$) = 3.3	Slot breadth/nozzle–wheel gap
$\Delta P = 50\,000$ dyn cm^{-2}	Applied pressure drop	T ($\equiv T/G$) = 0.3	Thickness/nozzle–wheel gap
Physical parameters of aluminium			
$\rho_l = 2300$ kg m^{-3}	Liquid density (1033 K)		
$\mu = 0.0010$ kg m^{-1} s^{-1}	Viscosity (1033 K)		
$\sigma = 0.86$ N m^{-1}	Surface tension (1033 K)		

1) are listed in Table I. Noticeably absent are parameters associated with the heat transport such as superheat, thermal conductivities, heat-transfer coefficient, etc. Indeed, the only parameter influenced by the thermal aspects of the process which appears is solidification rate. The other thermally related parameters are held fixed in the experiments and hence are not needed to characterize the process dependencies.

For the range of parameters typical of the process, the heat transfer is only weakly coupled to the fluid mechanics. Indeed, Chu *et al.* [9] measured the average solidification rate, H^*, and found it to be essentially independent of ribbon thickness for fixed thermal conditions. Furthermore, the non-dimensional solidification rate $H = H^*/U$, which corresponds to an average slope of the solidification front, is very small ($H \ll 1$) over the range of wheel speeds of interest to rapid solidification application. This suggests that to a first approximation, H can be taken as constant and equal to zero. Nevertheless, for completeness, we include H in the set of dimensionless parameters even though experiments show below that the thickness is independent of H within experimental error. The precise asymptotic limits of the full heat and momentum equations for which the decoupling occurs are developed by Carpenter [10].

Turning to the fluid mechanics, Table I shows that inertial forces are generally very large relative to surface tension forces (Weber number $\gg 1$) and very, very large relative to viscous forces (Reynolds number $\gg 1$). It is therefore reasonable to take the first-order balance to be between inertia and the pressure force. Note that a Reynolds number based on mass flow rate is less than half that listed (Table I) and with the stabilizing influence of a sink of mass at the solidification interface, the flow state may not be turbulent. The physics can be better appreciated by considering the corresponding asymptotic limits of the full energy and momentum equations [10].

By the above arguments the relevant parameters can be reduced to a set of eight (ΔP, U, ρ, T, G, R, W, H^*) which may be arranged in the following non-dimensional groups (cf. Pi theorem): $(\Delta P/\rho U^2)$, (T/G), (R/G), (W/G), H. The width of the ribbon is much greater than any other length scale in the problem, so the variations in ribbon thickness from changes in (W/G) are expected to be negligible. This is indeed confirmed by experiment below and supports the simplification made in most analyses where the fluid mechanics equations are reduced to two dimensions [11–14]. Isolating the thickness as a preferred parameter leaves a functional framework within which the experiments are expected to fit

$$(T/G) = \Phi[(\Delta P/\rho U^2), (R/G), (W/G), H] \quad (2)$$

With the exception of H and W/G, the parameters included in this analysis are similar to those used in previous experimental analyses [4–8].

3.2. Operating limits

Note that the only material parameter to appear in the steady-state functional dependence is the metal density (Equation 2). Yet, it is surface tension which holds the metal between the nozzle face and the spinning wheel. If surface tension effects were not important, an infinite range of pressure drops and wheel speeds with the same ratio of pressure to inertial forces would deliver the same ribbon thickness, once the geometry is fixed. This is not true. For some pressure drops and wheel speeds, metal will not flow out at all, while for others with the same ratio of pressure to inertial forces, a uniform ribbon results as outlined in Section 1. Clearly, surface tension effects must be included when considering stability of the process. Additional parameters may also enter. For example, the width of the nozzle slot, which is not expected to influence steady-state behaviour, may affect stability. A set of dimensionless groups sufficient to characterize the process stability will therefore include at least surface tension, σ, and nozzle width, W.

The maximum pressure jump which can be sustained by the upstream meniscus of the metal bead formed between the nozzle face and spinning wheel is

$$\Delta P_{max} = 2\sigma/G \quad (3)$$

If the pressure drop and inertial forces are non-dimensionalized by this "blow-out" pressure, the following set of operating parameters are proposed as relevant to determining the operating window in which a uniform ribbon may be produced: $[\Delta P/(2\sigma/G)]$, $[\rho U^2/(2\sigma/G)]$, (R/G), (W/G), H.

A systematic way to understand how these parameters characterize operating limits on the planar-flow process is through a plot (Fig. 7) of the inertial parameter, $\rho U^2/(2\sigma/G)$, versus the pressure parameter, $\Delta P/(2\sigma/G)$. In this graph each straight line which passes through the origin represents a point from the non-dimensional steady-state space of the system. Along each line $\Delta P/\rho U^2$ is constant, and a uniform ribbon is produced for this ratio of pressure and inertial forces only when both the pressure and inertial operating parameters are between their high and low threshold values. For each line (i.e. each value of $\Delta P/\rho U^2$) the length of this range may vary, and for different values of R/G, W/G, and H a different operating range may be found.

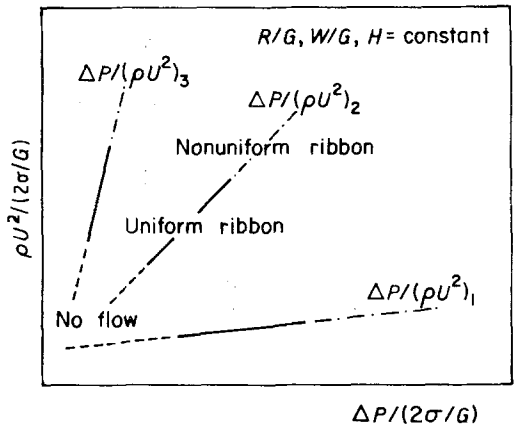

Figure 7 Schematic operating limit plot.

4. Quantitative results

4.1. Steady-state dependence

The raw data with assigned run numbers are listed in Table II. After illustrating the reproducibility of the raw data, confirmation of the reductions dictated by dimensional analysis is illustrated and then experimental evidence that thickness is independent of (W/G) and H is summarized. The main topics of this section, correlation of our data and a composite plot with data from the literature, then follow.

The reproducibility of raw data is estimated from two pairs of runs; for each pair the processing conditions are essentially identical. The first pair correspond to Runs 12 and 13 (Table II) and produced ribbons of thickness 188 and 186 μm, respectively. The difference between the non-dimensional thicknesses (T/G) is 2%. The second pair correspond to Runs 30 and 33 (Table II) and deliver thicknesses of 167 and 186 μm, respectively. Here, the difference between the non-dimensional thickness values is 7%. While the first result is more satisfying, the second result is a better indication of the true reproducibility of the system.

The reproducibility of the experimental apparatus is limited by the measurement of the gap between the nozzle face and the chill wheel. The optical telescope used to measure the gap is accurate to within 0.002 54 cm (0.001 in.) which is less than 5% of the gap size, but the ability of the observer to measure this distance is not as great as the instrument's precision. To measure the gap the crosshairs of the telescope lens must be lined up with the wheel surface and then the nozzle face. Repeated measurements of the gap show that the reproducibility of this measurement is between 0.005 cm (0.002 in.) and 0.0076 cm (0.003 in.). This error is between 5% and 8% of the usual gap size, and this is the error size found in the second test of reproducibility.

To confirm that the non-dimensional groups characterize the state of the system, ribbons were made under similar non-dimensional parameters but different dimensional process conditions. Runs 20 and 22 have different dimensional parameters but the same dimensionless groups (Table III). The non-dimensional ribbon thicknesses are only 3.4% different. The error in the results is easily accounted for by the experimental error in the system.

The ribbon thickness also shows little or no dependence on the non-dimensional slot width (Runs 20 and 22). To illustrate this further, a pair of ribbons, Runs 26 and 28, were made under similar conditions, but with nozzle slots of different widths (Table IV). The non-dimensional thicknesses are 9% apart, just above the reproducibility of the system.

Furthermore, we note that data reported in the literature from other systems (see below) compares favourably with our data under the similarity of the dimensionless groups. Here, "favourably" takes into account that the error in other systems is difficult to determine because of limited information but may be as high as 20% in some cases. As far as dependence on slot width is concerned, comparisons drawn below among systems from four different groups corresponding to ribbons which range in width from 10–50 mm shows there is no discernable dependence of thickness (T/G) on width (W/G).

The thickness is also independent of H within the error of the experiments. Indeed, if H^* is assumed to be constant (26 cm s^{-1} according to [9]) or nearly constant, then H ($\equiv H^*/U$) varies by 28% between Runs 20 and 22, for example, but the thickness (T/G) remains unchanged between these runs. Broadly speaking, the group H is not needed to correlate the data. On the other hand, there are clearly operating conditions where the heat transfer limits the operation, as illustrated below in the discussion of "heat-up"

TABLE II Experimental results

Run no.	U (cm s^{-1})	ΔP (dyn cm^{-2})	T (μm)	G (μm)	R (μm)	W (in.)
1	964	40 700		508	3180	2.0
2	980	48 300	171	635	3180	2.0
3	808	47 800		508	3180	2.0
4	782	67 900	230	635	3180	2.0
5	648	67 300	209	584	3180	2.0
6	508	67 100		533	3180	2.0
7	737	59 900	244	508	3180	2.0
8	1117	63 200		559	1590	1.0
9	1149	61 400		686	1590	1.0
10	1388	60 700	118	711	1590	1.0
11	977	60 900	158	737	3180	2.0
12	951	60 600	188	991	3180	2.0
13	954	60 700	186	965	3180	2.0
14	964	48 800	193	1168	3180	2.0
15	983	59 900	176	940	3180	2.0
16	989	47 600	149	940	1590	2.0
17	664	48 700	174	940	1590	2.0
18	1277	48 500		965	1590	2.0
19	539	48 500	217	940	1590	2.0
20	1133	62 550	110	630	1590	2.0
21	919	40 800		1270	3180	2.0
22	823	32 900	224	1240	3180	2.0
23	642	48 600	294	940	3180	2.0
24	1347	58 000	133	787	3180	2.0
25	753	48 500	194	953	3180	2.0
26	808	48 600	175	940	1590	1.0
27	1296	48 100	128	940	1590	1.0
28	801	48 000	160	940	1590	2.0
29	555	42 700	231	940	1590	2.0
30	814	53 800	167	635	3180	2.0
31	616	53 700	234	660	3180	2.0
32	932	78 600	205	635	3180	2.0
33	814	53 900	186	660	3180	2.0
34	600	39 800	221	1016	3180	2.0

TABLE III

	$\Delta P/\rho U^2$	R/G	W/G	T/G
Run 20	0.021	2.53	31.95	0.175
Run 22	0.021	2.55	15.97	0.181

TABLE IV

	$\Delta P/\rho U^2$	R/G	W/G	T/G
Run 26	0.032	1.7	15.97	0.186
Run 28	0.033	1.7	31.95	0.170

of the wheel. In these cases, H^* becomes sufficiently small that solidification no longer occurs.

The data from our system with corresponding error bars are plotted in Fig. 8 as (T/G) versus $(\Delta P/\rho U^2)$ with (R/G) as parameter. Data with the same breadth are plotted using the same symbol. The influence of increasing breadth (R/G) is an increase in the thickness (T/G), as expected, because for fixed pressure drop, larger entrance channels favour greater mass flow rates. Furthermore, increasing pressure drop $(\Delta P/\rho U^2)$ leads to greater thickness (T/G) for fixed slot breadth (R/G), as expected. These observations confirm trends reported in earlier studies. More interesting is the observation of a similarity in the functional relationship (T/G) versus $(\Delta P/\rho U^2)$ for various breadths. This similarity is discussed further after describing how the curves in Fig. 8 were obtained.

For each value of (R/G), the data in Fig. 8 are fit to the equation

$$(T/G) = a(\Delta P/\rho U^2)^b \quad (4)$$

A least squares analysis determines the unknown constants a and b. The constants and their respective errors for the three values of R/G are given in Table V. The errors listed for each of the values are the best estimate of the standard deviation (BESD) and the value and the errors for a and b define an envelope in which approximately two-thirds of the data would be found [15]. The value for R/G excludes the point at large pressure which gives a much greater thickness (Fig. 8). If this point is included, a and b for $R/G = 3.3$ are 1.51 ± 1.07 and 0.59 ± 0.20, respectively. A curve is drawn for each of these four values of a and b in Fig. 8. There is some evidence that a hydrodynamic transition occurs for large pressure drops and the deviant point may result from a flow that has undergone transition [16].

The general similarity of the curves (cf. exponents b) are especially evident if the maverick point is excluded. A mass balance combined with an elementary Bernoulli balance for the flow in the wheel/nozzle gap predicts

$$(\Delta P/\rho U^2) \propto (T/G)^2 \quad (5)$$

The deviation of the exponents b from the value 1/2 suggests that the flow geometry, and in particular, the length of the solidification front, may depend on the pressure drop and wheel speed in a non-trivial way. Nevertheless, the proximity of the exponents b for three values of (R/G) suggests that a modified law holds with a constant of proportionality that depends on (R/G). In view of the experimental error, more definite conclusions are inappropriate. Several earlier studies have reported $b = 0.5$ correlations over at least a range of applied pressures, but the range of pressures has been only a fraction of that reported here (cf. Fig. 9) which may account for the discrepancy [5, 7].

TABLE V

R/G	a	b
1.7	0.52 ± 0.09	0.31 ± 0.05
3.3	0.48 ± 0.18	0.26 ± 0.06
5.0	0.83 ± 0.23	0.31 ± 0.08

The experimental data from our system are compared with data from three previous works in Fig. 9. The published data are from Huang [5], Fiedler *et al.* [7], and Smith and Saletore [8]. The metal used by Huang, and Smith and Saletore was an iron alloy, and the metals used by Fiedler *et al.* were an iron alloy and an alloy containing a one-to-one mixture of iron and nickel. The alloys used in the three published sets of data contained some non-metallic components. Because the non-metallic part made up no more than 20% of any of the alloys, the density was determined

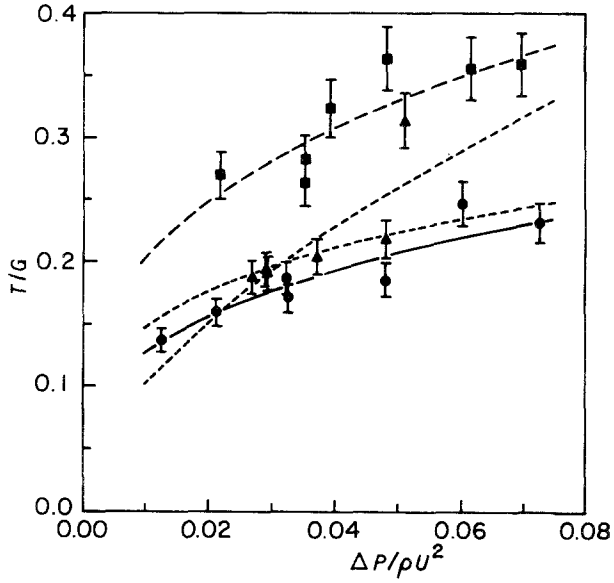

Figure 8 Experimental result plot. R/G: (– – ■– —) 5.0, (– – – – ▲– – – –) 3.3, (—●—) 1.7.

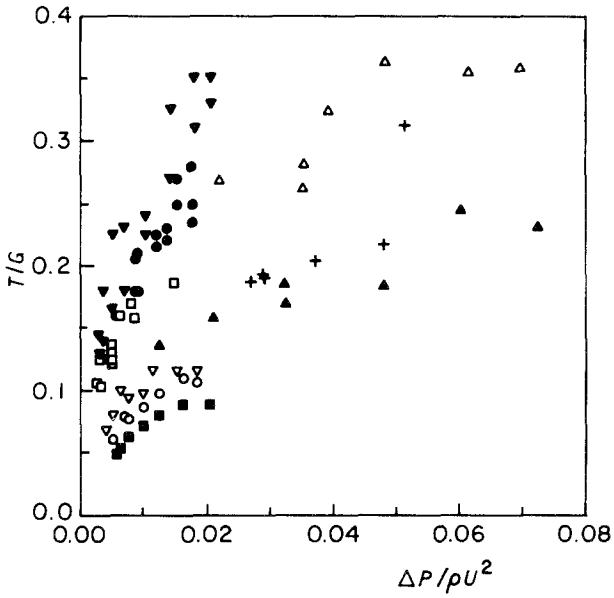

Figure 9 Combined plot. R/G: (▼) 5.5 ([7] Fe); (△) 5.0 (present work, Al); (●) 4.0 ([7] Fe/Ni); (□) 3.5 ([8] Fe); (+) 3.3 (present work, Al); (▽) 2.5 ([5] Fe); (▲) 1.8 (present work, Al); (○) 1.7 ([5] Fe); (■) 1.1 ([5] Fe).

using only the metallic part. The data presented by Smith and Saletore are the only ones in tabular form; the dimensional data in the other papers were obtained from plots of the results.

The experimental results correlate well within the experimental error of the different systems (Fig. 9). In all cases the thickness increases with increasing pressure drop and/or slot breadth. Points from different data sets show similar thicknesses under similar non-dimensional processing conditions. The only points which do not correlate well are Huang's data for large pressure drop relative to wheel speed. Instead of the thickness increasing with pressure drop for these points, the thickness levels off. Whether Huang's system was a planar-flow configuration or not has been questioned by Fiedler *et al.* who feel that the ribbon width may have had some effect on Huang's experiments [7]. This change in width is typical of the chill-block method. In all studies, the scatter in data is greater for larger (R/G) and larger thicknesses.

Much of the scatter in the data is due to experimental error and a lack of detailed information on the processing conditions for the ribbons reported in the literature. In some systems, data at constant values of ΔP, U, R, G and H show 10%–20% difference in the thicknesses. In addition, little or no information was provided in the published results on the size of the ingots cast, and how constant the ribbon thicknesses were along the length of the ribbon – no information was provided on the steadiness of the process. Furthermore, it should be noted that the literature results are from alloy systems, while the correlation is developed assuming the material is a pure metal.

Overall the experimental results correlate well for different metals. The non-dimensional ribbon thickness depends on only two dimensionless parameters, the ratio of pressure drop to inertial forces and the ratio of nozzle-slot breadth to nozzle/wheel gap. All other material properties and process conditions are of secondary importance in determining the final ribbon thickness.

4.2. Operating limits

During the experiments, if the non-dimensional operating limits of the system were exceeded, the following qualitative results would occur. If $\Delta P/(2\sigma/G)$, $\rho U^2/(2\sigma/G)$, or both, were below the operating minimum, metal would not flow out at all. Above the maximum operating value of the pressure parameter, $\Delta P/(2\sigma/G)$, surface tension would not hold the liquid puddle in place. The puddle (i.e. ribbon) became wider than the nozzle slot and the flow was non-uniform, as evident from the solidified product. When the inertial operating parameter, $\rho U^2/(2\sigma/G)$, was above its ceiling value, the liquid did not form a single, uniform puddle in the gap and, instead, separated into fingers of metal. Some of these fingers formed narrow ribbons and some metal came off the wheel without freezing at all.

There are insufficient data produced in this study to give an accurate picture of the regions which will or will not produce a uniform ribbon, but data that were produced show broad changes in the ability of the process to produce a uniform product. The pressure and inertial operating parameters are plotted in Fig. 10 for R/G values of 1.7 and 6.0. Points in the plots show whether the pressure parameter was exceeded, whether the inertial parameter was exceeded, whether there was no metal flow at all, or whether a uniform ribbon was formed. For purposes of demonstration, the value of H given is an average value for the data plotted. While H may influence the operating limit plots, in the data obtained so far H apparently does not have a large qualitative influence, similar to the situation discussed above for the steady-state dependence.

An important conclusion from the $R/G = 1.7$ data, is that although the width of the ribbon does not strongly affect its final thickness, it does control the range of processing parameters for which a uniform ribbon is obtained. Two runs (18 and 27) with different slot widths but otherwise identical conditions illustrate this. The operating parameters for these runs are given in Table VI. No ribbon was formed with the larger slot width (run 18); the metal shot off the wheel without freezing. Under similar conditions with a narrower slot (Run 27), a continuous ribbon was formed.

In summary, the operating parameters and operating limits of the planar-flow system are influenced by a larger set of parameters than the steady-state behaviour. These parameters are shown to include, for fixed thermal conditions, the metal surface tension, nozzle-slot width, and, possibly, the solidification rate.

TABLE VI

	$\Delta P/(2\sigma/G)$	$\rho U^2/(2\sigma/G)$	R/G	W/G
Run 18	2.62	211	1.7	270
Run 27	2.72	210	1.6	53

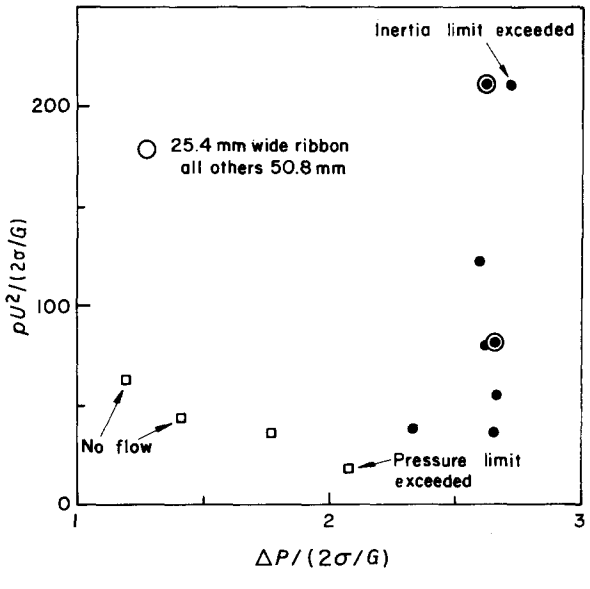

Figure 10 Operating limit plot. (□) $R = 6.0$, $H = 0.034$; (●) $R = 1.7$, $H = 0.030$.

5. Observations

5.1. Process

Both still photography and videorecording of the gap region yield qualitative information about the process behaviour. These images confirm that the upstream meniscus remains at or near the upstream side of the nozzle slot; there is little or no flow of the metal against the wheel direction. Although similar observations have been recorded in the literature, alloys such as mixtures of iron which have a much larger surface tension than aluminium, have been the typical working metal and gap sizes have been typically half as large as used here. Under such conditions, blow-out as well as movement against the wheel direction is suppressed.

A second observation concerns the tendency of the wheel to heat up for runs of longer duration. Runs which process 1.6–1.8 kg metal, were qualitatively different from those processing only 0.7–0.9 kg metal. Although in both cases the first 0.7–0.9 kg spun off in a similar manner, the ribbon thickness in the later half of the longer experiments was much smaller and near the end of the runs some metal was not quenched at all. Similar changes in thickness have been reported but generally have been attributed to expansion of the wheel (eg. [17]). We have been able to distinguish these two effects.

Generous estimates of the heating of the wheel suggest that the surface temperature can increase up to 50 K with every revolution. This order-of-magnitude estimate is probably larger than the actual heat-up. For a run of 0.7–0.9 kg, the wheel turns approximately 15 revolutions, and for a 1.6–1.8 kg run, this number is twice as large. If the temperature of the wheel increased 20 K with each revolution during the experiment, a short run would lead to a wheel surface temperature of approximately 325 °C. This would be significantly lower than the melting temperature of the aluminium, 660 °C, and the wheel could quench the metal. For a 1.6–1.8 kg run, however, the surface temperature would be approximately 625 °C, just below the melting point of aluminium, the wheel would no longer be able to readily freeze the metal. Similar rates of heat-up are cited by Huang and Fiedler for the chill-block process [18].

These findings are further supported and expanded by experiments on another planar-flow melt-spinning system [19]. There, the aluminium was superheated approximately 500 K above the melting point in order to dissolve an additional component into the aluminium. The wheel is unable to quench the metal in the same manner as with superheat of only 100 K. It was found, furthermore, that the relative widths of the wheel and ribbon also affect the heat-up of the wheel. In particular, when the width of the wheel is larger relative to the width of the ribbon, a longer ribbon is formed and the wheel acts as a better heat sink, as one might expect.

5.2. Ribbon surface textures

In planar-flow melt-spinning the ribbon surface not in contact with the wheel usually contains non-uniformities even under normal casting conditions. These textures appear to be a result of poor contact between the liquid metal and the chill wheel, as has been observed [6]. Here we catalogue surface textures found most often under steady-state conditions and suggest possible causes.

The first texture will be called "dimple pattern". This imperfection is made up of relatively large depressions found on the meniscus side of the ribbon which correlate with smaller depressions at the same location on the metal/wheel contact surface of the metal strip (Fig. 11). This texture is found on all experimental runs and is by far the most common non-uniformity. Depressions on the wheel side are caused by air entrainment when the liquid metal first contacts the wheel and lead to non-uniformities in heat transfer. The correlation with the dimple pattern on the upper surface has several possible explanations. At such locations in the puddle the metal is not solidifying as quickly and, therefore, the ribbon may be expected to be thinner. Alternatively, such points in the melt puddle will be locally hotter and may cause a decrease in the surface tension on the upper surface. A Marangoni instability may then ensue and ultimately be frozen into the ribbon.

The second texture will be referred to as the "streak pattern" (Fig. 12). This type of imperfection appears as long, thin grooves in the direction of casting on the upper surface of the ribbon. The cause of the streak pattern may be similar to the dimple pattern. On the wheel side of the ribbon thin lines of poor contact between the metal and the wheel are found. In addition to the mechanisms which affect the ribbon surface in dimpling, there is the possibility of enhancement of the streaks by a "painting" type instability, like that found in coating of thin films.

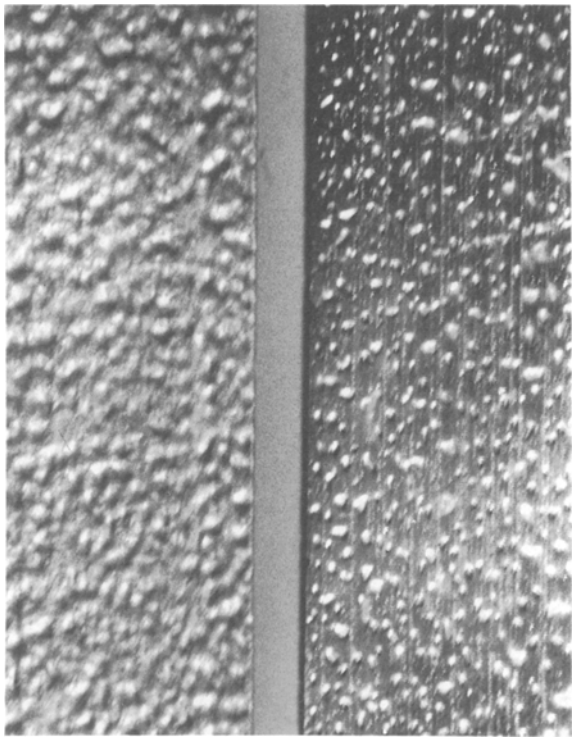

Figure 11 Dimple pattern.

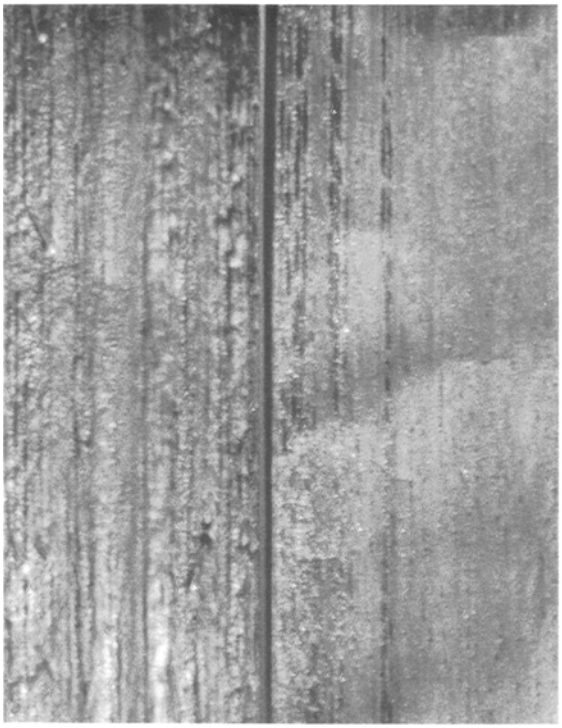

Figure 12 Streak pattern.

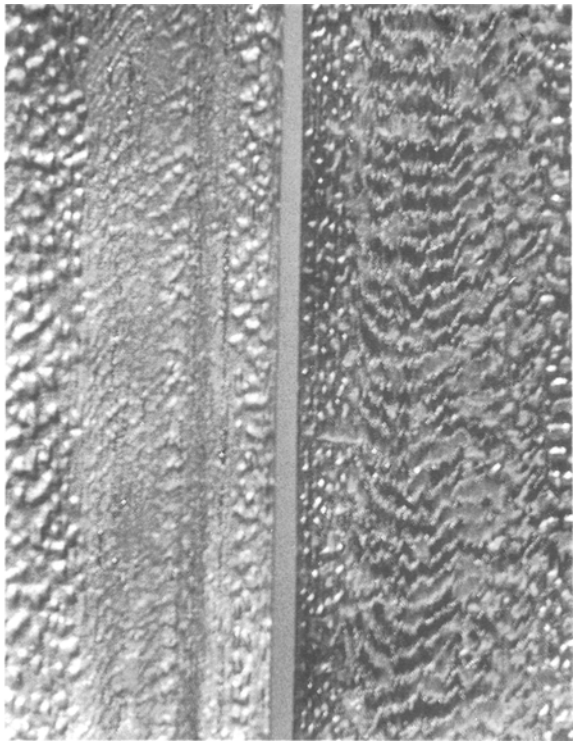

Figure 13 Herringbone pattern.

The last non-uniformity is the "herringbone pattern" found on the wheel contact side of the ribbon (Fig. 13). This imperfection is caused by small non-uniformities in the fluid flow. The herringbone texture would be found, typically, when a small piece of metal protrudes slightly into the nozzle slot flow path. Some of the liquid metal would flow around the protrusion causing the liquid metal to contact the wheel in a non-uniform manner and to produce a characteristic pattern in the solid ribbon. This pattern may be desirable in some cases because it suppresses other instabilities such as the dimple pattern. Although the herringbone pattern on the meniscus side of the ribbon is produced by a similar mechanism to the dimple pattern, the upper surface of the ribbon is smoother overall.

Finally, we note that under non-steady flow conditions, typically at the start of a run, non-uniform contact of the metal with the wheel can leave characteristic features similar in size to the dimple pattern but with deeper penetration. Often, contact at these points is so poor that little solidification takes place before the metal leaves the wheel. Instead, liquid metal is carried along by the surrounding solidified ribbon. After the ribbon leaves the wheel, this liquid metal solidifies leaving a very non-uniform protrusion on the free surface side of the ribbon. These imperfections are a useful indication of the uniformity of the flow in a given experiment. Under normal run conditions, this type of imperfection is only found at the start of the ribbon. However, if there is blockage of the flow path or other non-uniformity in the flow, this type of imperfection is found in other sections of the ribbon.

6. Conclusions

In order to understand the influence of mechanical parameters which control the planar-flow process, an apparatus which delivers reproducible results is required. The largest source of error as far as ribbon thickness is concerned is the precise control and measurement of the narrow gap (< 1 mm) between nozzle and wheel. The technical difficulties here are (i) that control and measurement must be made while the nozzle is hot (700 °C) to take account of significant thermal expansion of the graphite nozzle material, and (ii) that the gap must be maintained throughout the run withstanding the varying load due to discharge of up to 2 kg molten metal.

Design of our apparatus is described in some detail to show how attention to appropriate design elements address these difficulties. The end result is average ribbon thickness reproducible to within 5%–8%. The soundness of the basic design has been further confirmed by the fact that minor modifications subsequent to the experiments reported here have improved reproducibility to 2%–3% [16]. Perhaps more significant than the actual magnitude of error is the accounting of sources of error which allows assignment of error bars to the data.

This study focuses on the influence of mechanical as separate from thermal conditions. The observed weak coupling between heat-transfer and fluid mechanics at least for typical heating/quenching situations and for wheel speeds where rapid solidification is feasible makes such a separation possible.

Guided by principles of dimensional analysis and based on the magnitude of dimensionless groups typical of the process, the dominant fluid dynamic balance for steady behaviour is shown to be between applied pressure and inertia. This framework leads to successful correlation of our data and data from the literature. It is emphasized and confirmed by experiments, as far as they go, that the operating limits as well as the surface textures will depend on, in

addition, the surface tension, the nozzle width, and, perhaps, the solidification rate.

The thickness versus pressure drop data show a consistent functional form as they depend on nozzle breadth. Thickness varies with applied pressure to the 1/3 power, approximately, and with the wheel velocity to $-2/3$ power, approximately. Increases in nozzle breadth shift the curve to larger thicknesses. The error bars associated with the exponents are significant and the relatively small number of data points (due to a significant time/run) over a large range of applied pressures leaves questions about resolution of the curve. Because, with perfect resolution and no error, such a curve may well display changes in shape (e.g. due to flow transitions) over such a range of driving force (four times that of previous studies) the value of the exponents must be interpreted cautiously. Further experiments are needed.

The textures frozen into the top-side of the ribbon may be influenced by a number of effects including meniscus instabilities, flow instabilities and non-uniformities in heat transfer. Three of the textures most often observed under steady conditions are a dimple pattern, a streak pattern, and a herringbone pattern. Characteristic of all three are features on the wheel side of the ribbon which correlate in a one-to-one manner with the top-side pattern suggesting that heat-transfer effects are most probably responsible. Possible mechanisms are discussed.

Acknowledgements

Informative discussions with Drs Ho Yu and Men Chu, Alcoa Technical Center, are greatly appreciated. We also thank Chuck Agger for useful discussions. This work was mainly supported by NSF Grant MSM 8711824.

References

1. S. KAVESH, in "Metallic Glasses", edited by J. Gilman and H. Leamy (ASM, Metals Park, OH, 1978) p. 36.
2. H. JONES, in "Rapid Solidification of Metals and Alloys" (Institution of Metallurgists, London, 1982).
3. D. NARSIMHAN, US Pat. 4 142 571 (1979).
4. S. TAKAYAMA and T. Oi, *J. Appl. Phys.* **50** (1979) 4962.
5. S. C. HUANG, in "Rapidly Quenched Metals", Vol. IV, edited by T. Masumoto and K. Suzuki, (Japan Institute of Metals, Sendai, 1981) p. 65.
6. S. C. HUANG and H. C. FIEDLER, *Met. Trans.* **12A** (1981) 1107.
7. H. FIEDLER, H. MUHLBACH and G. STEPHANI, *J. Mater. Sci.* **19** (1984) 3229.
8. M. T. SMITH and M. SALETORE, *Rev. Sci. Instrum.* **57** (1986) 1647.
9. M. G. CHU, A. GIRON, and D. A. GRANGER, in "Proceedings of the International Conference on Rapidly Solidified Materials" (ASM, Metals Park, OH, 1986) p. 311.
10. J. K. CARPENTER, PhD thesis, Cornell University, Ithaca, NY (1990).
11. H. YU, *Met. Trans. B* **18** (1987) 557.
12. P. H. STEEN, H. YU and J. K. CARPENTER, *AIChE J.* **34** (1988) 1673.
13. E. M. GUTIERREZ and J. SZEKLEY, *Met. Trans. B* **17** (1986) 695.
14. S. A. BERGER, and D. K. Ai, *ibid.* **19** (1988) 571.
15. P. E. FIELD, "Physical Methods in Chemistry" (Virginia Polytechnic Institute and State University, Blacksburg, VA, 1982).
16. E. C. AGGER, Private Communication.
17. M. J. FLEETWOOD, A. G. LAW, J. E. WHITTLE, A. G. TODD and J. H. VINCENT, in "Proceedings of the 2nd Conference on Rapidly Solidified Materials: Properties and Processing", San Diego, CA, edited by Peter W. Lee and John H. Moll (ASM International, Metals Park, OH, 1988) p. 115.
18. S. C. HUANG and H. C. FIEDLER, *Mater. Sci. Engng* **51** (1981) 39.
19. M. G. CHU and D. A. GRANGER, private communication (1989).

Received 3 September
and accepted 19 November 1990